Supporting Information for "Monitoring Preferential Flow Distribution in Sand Using Thermoacoustics Wave Imaging Methods"

Chang Liu [1] [*], Xu Mao [1], Chang Wang [1], Rebecca Liyanage [2], Juan Heredia

Juesas [1,3], Ruben Juanes [2], Jose Angle Martinez-Lorenzo [1,3] [†]

[1]Department of Mechanical and Industrial Engineering, Northeastern University, Boston, Massachusetts, 02115

[2]Department of Civil and Environmental Engineering, Massachusetts Institute of Technology, Cambridge, Massachusetts, 02139

[3]Department of Electrical and Computer Engineering, Northeastern University, Boston, Massachusetts, 02115

Contents of this file

1. Text S1 to S8

2. Figures S1 to S5

3. Table S1

Additional Supporting Information

1. Caption for Movie S1

———————

[*]liu.chang4@northeastern.edu

[†]j.martinez-lorenzo@northeastern.edu

December 21, 2022, 2:09am

Introduction This *supplementary materials document* describes our computational simulation model, experimental testbed, data processing pipeline, and imaging algorithm used to generate the results presented in the letter. Moreover, a data repository has been made publicly available to ensure reproducible results. The letter proposes to apply the microwave-induced thermoacoustics imaging (TA) method to reconstruct the water infiltration process in the porous sand. Firstly, a simulation is conducted to establish the relationship between the TA signal strength and the saturation levels. The rock physics model (RPM) used in the simulation is introduced in Text S1, and the simulation model is described in Text S2. Afterward, an experiment is conducted to validate the simulation results. The TA signals generated by sand boxes with different saturation levels are collected in this experiment. The pressure data is converted by the transducer to a voltage signal and collected through an ultrasound receiver at a gain of 79dB. The testbed and experiment process are described in Text S3. Based on the aforementioned results, the finger infiltration experiment can be conducted, and this experiment process is described in Text S4. The data collection system of the finger imaging experiment is similar to that of the sand box experiment. A raster scan is conducted after each experiment stage is finished. The data processing method is described in Text S5, and the imaging algorithm is given in Text S6. It is noticed that the original reconstructed image is in the unit of image strength. However, such information can be used to infer the water saturation level in sand based on the established relationship between the water saturation level and the TA amplitude. This theory is explained in Text S7. Finally, the slow scanning limitations of the current testbed is explained in Text S8.

Text S1.

Rock physics model used for the computational simulations

A RPM is used to derive the relationship amongst the electromagnetic constitutive properties from rock morphology and fluids distribution in a porous media. The complex dielectric constant ϵ_c is usually expressed as the combination of relative permittivity ϵ_r and electric conductivity σ, as shown in Eq. (1a). The relationship between the porosity Φ (assuming fully saturated) and the complex dielectric constant ϵ_c in saturated sand can be modeled by the Bruggerman-Hanna-Sen formula (Shen et al., 1985), which is given in Eq. (1b):

$$\epsilon_c = \epsilon_r - j\frac{\sigma}{\omega_e} \tag{1a}$$

$$\Phi = \frac{\epsilon_c - \epsilon_{c2}}{\epsilon_{c1} - \epsilon_{c2}\left(\frac{\epsilon_{c1}}{\epsilon_c}\right)^{\frac{1}{3}}}, \tag{1b}$$

where ω_e is the angular frequency of the EM wave, the subscript $[\cdot]_1$ denotes properties of water, $[\cdot]_2$ stands for the properties of dry quartz sand, and $[\cdot]$ for the water-saturated sand. Moreover, the rock physic models of the thermal expansion coefficient β (Troschke & Burkhardt, 1998) and specific heat capacity C_p (Waples & Waples, 2004) are given in Eqs. (2a) and (2b), respectively:

$$\beta = \frac{(1-\Phi)\kappa_2\beta_2 + \Phi\kappa_1\beta_1}{(1-\Phi)\kappa_2 + \Phi\kappa_1} \tag{2a}$$

$$C_p = \frac{1}{\rho_2}(\rho_2 C_{p2}(1-\Phi) + \rho_1 C_{p1}\Phi), \tag{2b}$$

where κ is the bulk modulus, ρ is the density, and the meanings of the subscripts are identical as in Eq. (1).

Text S2.

Signal strength simulation

This simulation seeks to establish the relationship between the water saturation level in the sand sample and its corresponding TA signal amplitude using the selected RPM. The 3D profile of the simulation model, which is identical to the experiment geometry, is described in Fig. S1. A rectangle waveguide filled with air is applied to excite the 1.3GHz microwave, and its dimension is $165mm \times 100mm \times 82.5mm$, the same as the WR650 waveguide used in the experiment. Moreover, the PEC (perfect electric conducting) boundary condition is specified at the waveguide, as indicated by the orange line in Fig. S1. The sand sample, whose dimension is $30mm \times 30mm \times 13mm$, is immersed in oil and lifted 40mm from the acrylic sheet layer. The scattering condition (red line in Fig. S1) is assigned to the oil boundary to mimic the PML (perfectly matched layer) conditions. The simulation is conducted using the COMSOL-Matlab client (V5.2).

The relationship between the water saturation level and the signal strength is evaluated by two parameters: the source strength and the peak-peak amplitude. The source strength is defined as $S(\mathbf{r}) = -\frac{\beta(\mathbf{r})}{C_p(\mathbf{r})}\sigma(\mathbf{r})||E^2(\mathbf{r})||$, in which $\beta(\mathbf{r})$ is the thermal expansion rate, $C_p(\mathbf{r})$ is the specific heat capacity, $\sigma(\mathbf{r})$ is the electric conductivity, and $E(\mathbf{r})$ is the electric field. The source strength is computed by treating the sand box as a monopole source, and the volume average of the target is applied. Meanwhile, in order to compute the peak-peak amplitude, the sand box can be discretized into N_b elements with $S(\mathbf{r}_i)$ denoting the source strength for each element. Equation 3 is applied to obtain the received pressure profile $p(\mathbf{r}, \omega_a)$, in which ω_a and k_a are the angular frequency and wave number of the TA wave, separately. The corresponding peak-peak amplitude is obtained after the inverse Fourier operation of $p(\mathbf{r}, \omega_a)$.

$$p(\mathbf{r}, \omega_a) = \sum_{i=1}^{N_b} \frac{S(\mathbf{r}_i)}{|\mathbf{r} - \mathbf{r}_i|} e^{-jk_a|\mathbf{r}-\mathbf{r}_i|} \qquad (3)$$

Text S3.

Sand box experiment

This experiment is conducted to validate the relationship between the water saturation level and the corresponding TA amplitude. The system for measuring the TA signals generated by the sand boxes with different saturation levels is shown in Fig. S2a. A pulse lasting $1\mu s$ with 250Hz repetition rate is generated by the trigger source (Siglent SDG6000), and the microwave of 1.3GHz is excited by the microwave source (Hittite HMC-T2770). These two signals are transmitted through the microwave amplifier (AR 8000SP1z2G1z4M3), reaching a power of 2kW. The sand sample is placed in an oil bath, and the microwave is excited through a waveguide (WR650) to illuminate the sand box. A single-element transducer (Olympus A301) is used to collect the generated TA signal from the sand sample. Later, the TA signal is filtered by the ultrasound receiver (JSR DPR300) and displayed on an oscilloscope. The cable connection pattern for the devices is shown in Fig. S2b.

Text S4.

Water distribution imaging experiment

The experiment of water distribution imaging investigates the process of water infiltration into the dry sand cell using our proposed TA imaging techniques. The TA signal excitation system remains the same as the sand box experiment, but different transducer scanning platform and samples are used. As seen in Fig. S3a, the transducer is assembled on a

2D scanning platform that can run a raster scan in the X-Y plane. The linear encoder is also applied to the motion system, and a closed-loop control pattern is programmed to guarantee the precise measurement location. Moreover, the scanning platform also guarantees close contact between the transducer and the oil tank. The waveguide is placed at the back side of the sand cell, as shown in Fig. S3b. Figure S3c plots the sand sample from the top view. Two sand enclosures are prepared, and the thickness of the sand enclosure, which is 6.5mm, is smaller than the thickness of the sand cell. Moreover, the sand enclosure is closely attached to the front boundary of the sand cell, leaving no space for the air gap.

The temporal evolution of the water infiltration process is shown in Fig. S4. The fully saturated sand in the left enclosure is prepared as the reference marker, as displayed in Fig. S4a. For the first stage of this experiment, 1.5mL blue-dyed water is injected from the top into the right enclosure, and the water concentrates on the top of the enclosure, as shown in Fig. S4b. In order to avoid the Doppler effect, the raster scan of the transducer is conducted after the water profile stops developing. For the second stage of this experiment, three separate injections are attempted to fully saturate the right enclosure. The time separation between each injection and the injected water amount is presented in Table S1. Figures S4c-e show the photos for each separate injection in the second stage. It is observed that water goes to the bottom of the enclosure right after the first injection. The enclosure is sealed at the bottom, and this makes the fully saturated region to grow from the bottom to the top every time a new injection is made. Figure S4e shows the achieved fully saturated enclosure at the end of the experiment.

Text S5.

Data processing

The pressure profile of the received TA wave is converted to a voltage signal by the transducer and filtered by the ultrasound receiver. The transducer is fixed in the sand box experiment, and the TA pressure is measured at only one position. For the second experiment, the transducer conducts a raster scan for the dry sample, the fully saturated control marker enclosure on the left, and the two stages injecting water on the right enclosure. Thus, 4 sets of data are obtained for the second experiment. The collected data is named by the position of the transducer where it is measured. The amplifier power is also recorded to compensate for the power oscillation during the scan. The marker's image is obtained based on the difference between the dry sand and the marker. While the dynamic water distribution image is reconstructed based on the difference between the marker and the data collected in the corresponding experiment stage. Due to the mechanical misalignment, there is a sub-millimeter bias error in the Z-axis direction during the mechanical scanning. Hence, a compensation is made based on the arrival of the first peak in the measurement, which is generated by the front boundary of the sand cell. Moreover, a Hanning window is applied in the image reconstruction process.

Text S6.

Imaging method

The algorithm we used to reconstruct the image is derived from the governing equation Eq. (4). It is necessary to point out that Eq. (4) assumes that that the TA wave travels in an inelastic medium. The propagation of TA waves in the sand is not considered in the

experiment of the letter. This assumption only holds when the propagation distance in the sand is small compared to the distance between the sand sample and the transducer. For the other situations where the TA wave travels a long distance inside the porous medium, Eq. (4) will be invalid, and the effects of velocity dispersion and amplitude attenuation should also be considered when transforming the equation to the frequency domain.

$$\nabla^2 p(\mathbf{r}, t) - \frac{1}{c^2(\mathbf{r})} \frac{\partial^2}{\partial t^2} p(\mathbf{r}, t) = -\frac{\beta(\mathbf{r})}{C_p(\mathbf{r})} \frac{\partial Q(\mathbf{r}, t)}{\partial t} \tag{4a}$$

$$Q(\mathbf{r}, t) \approx \sigma(\mathbf{r}) ||E(\mathbf{r})||^2 f^2(t) \tag{4b}$$

Equation 4 can be written in the frequency domain as follows:

$$\nabla^2 P(\mathbf{r}, \omega_a) + k(\mathbf{r}, \omega_a)^2 P(\mathbf{r}, \omega_a) = -j\omega_a \frac{\beta(\mathbf{r})}{C_p(\mathbf{r})} \sigma(\mathbf{r}) ||\mathbf{E}(\mathbf{r})||^2 (F(\omega_a) * F(\omega_a)), \tag{5}$$

where $P(\mathbf{r}, \omega_a)$ is the TA pressure field in the frequency domain, and ω_a and $k(\mathbf{r}, \omega_a)$ are the angular frequency and the wave number of the TA wave, respectively. $F(\omega_a)$ is the Fourier transform of the time domain modulation signal $f(t)$, and $F(\omega)*F(\omega)$ refers to the convolution of $F(\omega)$ with itself. Meanwhile, Eq. (5) can be regarded as an inhomogeneous Helmholtz equation, and the solution can be written as follows:

$$\frac{j}{\omega_a} \frac{P(\mathbf{r}, \omega_a)}{F(\omega_a) * F(\omega_a)} = \int_V G(\mathbf{r}, \mathbf{r}', \omega_a) \frac{\beta(\mathbf{r}')}{C_p(\mathbf{r}')} \sigma(\mathbf{r}') ||E(\mathbf{r}')||^2 d\mathbf{r}' \tag{6}$$

where $G(\mathbf{r}, \mathbf{r}', \omega_a)$ is the unknown heterogeneous Green's function. A common assumption is to replace the Green's function $G(\mathbf{r}, \mathbf{r}', \omega_a)$ with the a known background approximation of the Green's function $G_b(\mathbf{r}, \mathbf{r}', \omega_a)$, which is computed in the absence of the target.

According to Eq. (6), it is reasonable to suggest that the TA amplitude is directly proportional to the source term $\frac{\beta(\mathbf{r})}{C_p(\mathbf{r})} \sigma(\mathbf{r}) ||\mathbf{E}(\mathbf{r})||^2$. In addition, the left-side operation of Eq. (6) guarantees that the reconstructed source term is independent of the modulation

signal. In this regard, different excitation patterns have been studied to improve the SNR (Signal to Noise Ratio) of the TA wave measurements. In order to solve Eq. (6), the imaging domain is discretized into $N = N_{row} \times N_{col}$ pixels, where N_{row} and N_{col} represent the number of pixels in rows and columns, separately. Correspondingly, the measurements $\mathbf{b}$ are collected by N_{rcv} receivers sampled at N_{fr} frequencies. Hence, the total number of measurements is $M = N_{rcv} \times N_{fr}$. The sensing matrix $A \in C^{(M \times N)}$ is composed of a discretization of the background field's Green's function. Hence, Eq. (6) can be written in the following form:

$$\mathbf{A}\chi = \mathbf{b}, \tag{7}$$

where $\chi = \frac{\beta(\mathbf{r}_n)}{C_p(\mathbf{r}_n)}\sigma(\mathbf{r}_n)||E(\mathbf{r}_n)||^2 (n = 1, 2, 3, ..., N)$ represents the unknown contrast variable discretized in the imaging domain. In a typical imaging scenario, the number of measurements is usually less than the number of unknowns, namely $M < N$, making that Eq. (7) has non-unique solutions. In this work, a complex conjugate pseudo-inverse approach is used to get the value of contrast variable.

Text S7.

Estimation of the water saturation level

The original images sliced at $Z = 118$mm for the marker, first injection, and last injection are shown in Figs. S5a-c, separately. It is observed that these images have identical profiles to the estimated water distribution results, which are presented in Figs. S5d-f, except the colorbar. Several assumptions made here to estimate the water saturation level in the sample. First, the relationship between the signal strength and water saturation level is approximated as a linear relationship for the sand box experiment. Second, the

water saturation level in the marker is assumed to be 100% for the ground truth. The bottom part of the last injection is also treated as fully saturated. Fourth, the area of water-saturated sand also affects the image strength, which leads to the maximum image strength of the marker being more significant than that of the second injection. Such area factor is also compensated in the process of saturation level estimation.

Text S8.

Scanning Speed

Although the purpose of proposing the application of TA imaging is to conduct real-time imaging, the scanning process of the water distribution imaging experiment takes about one hour. A video showing the scanning speed is uploaded as part of the supplementary material. As shown in Movie S1, there are two reasons leading to the slow scanning speed. The first one is that only one transducer is used in the experiment, thus requiring a raster mechanical scan of the target. Another reason is that the time spend by the transducer at each position is about 2s, so that the signal to noise ratio can be improved by averaging samples. Therefore, the total scanning time is around 1h, considering the number of measurement points is 729 and the slow-moving speed of the transducer. In the future, other acoustics real-time imaging techniques, such as a multi-element transducer, will be applied to increase the scanning speed, and the maximum image frame rate should reach 0.5Hz.

Movie S1. The transducer conducting a raster scan during the experiment.

References

Shen, L., Savre, W., Price, J., & Athavale, K. (1985). Dielectric properties of reservoir

rocks at ultra-high frequencies. *Geophysics*, *50*(4), 692–704.

Troschke, B., & Burkhardt, H. (1998). Thermal conductivity models for two-phase systems. *Physics and Chemistry of the Earth*, *23*(3), 351–355.

Waples, D. W., & Waples, J. S. (2004). A review and evaluation of specific heat capacities of rocks, minerals, and subsurface fluids. part 1: Minerals and nonporous rocks. *Natural resources research*, *13*(2), 97–122.
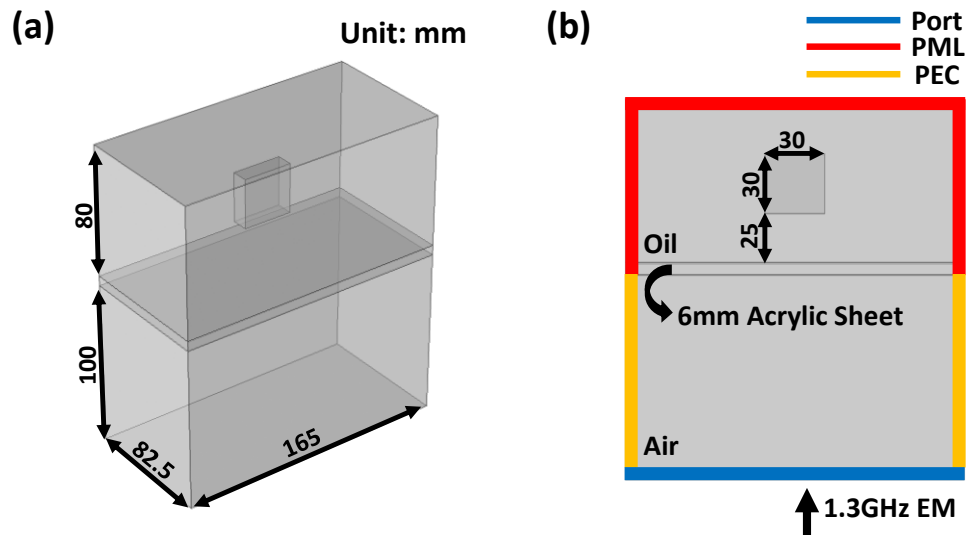
Figure S1. Simulation geometry for the relationship between signal strength and water saturation level: (a) geometry dimensions, and (b) boundary conditions
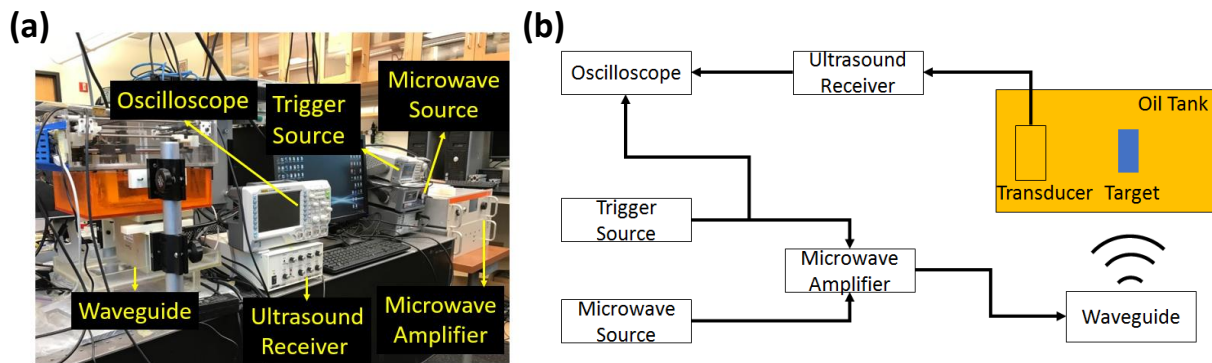

Figure S2. The testbed used to measure the TA signal generated by the sand box: (a) devices, and (b) the cable connection pattern.
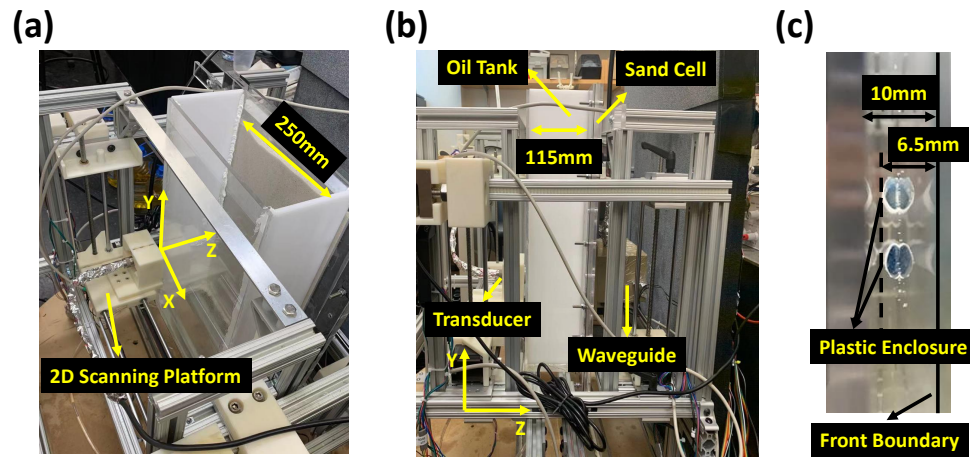
Figure S3. The testbed used to reconstruct the water distribution profile: (a) perspective view, (b) side view, and (c) the sand sample (top view).
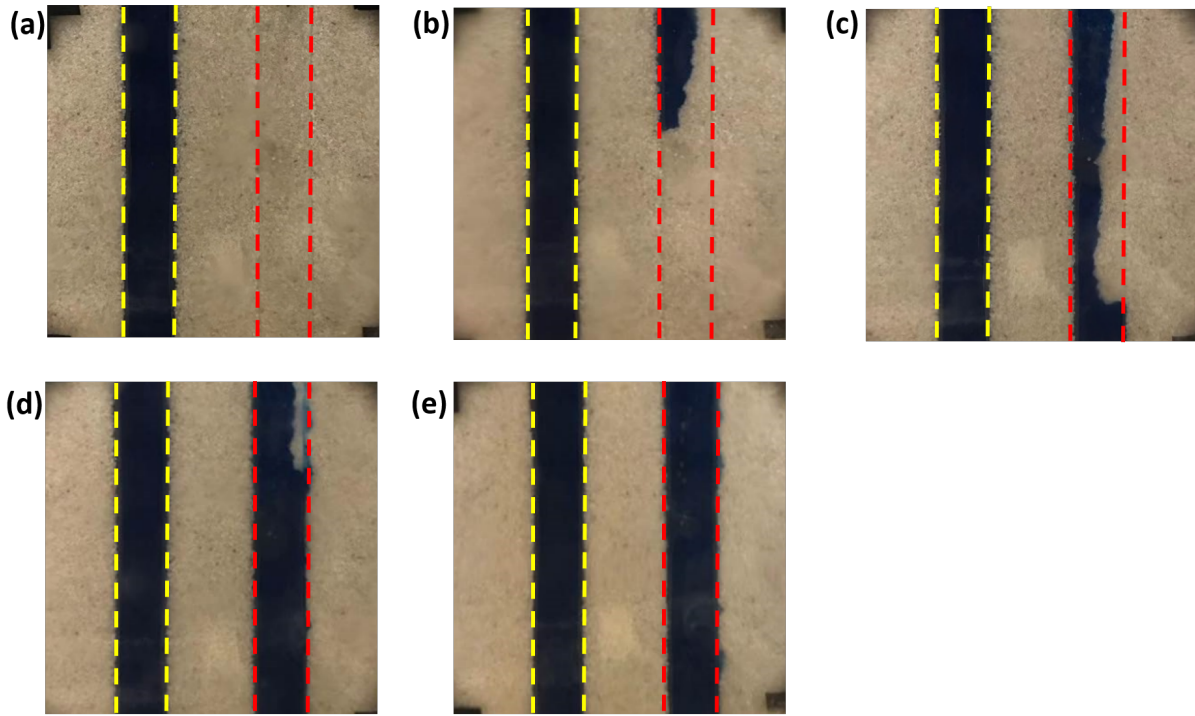
Figure S4. The water infiltration process: (a) the water distribution inside the marker (yellow dashed line), (b) the water distribution of the first stage experiment, the water distribution of the first (c), second (d), and third (e) injection in the second stage experiment.
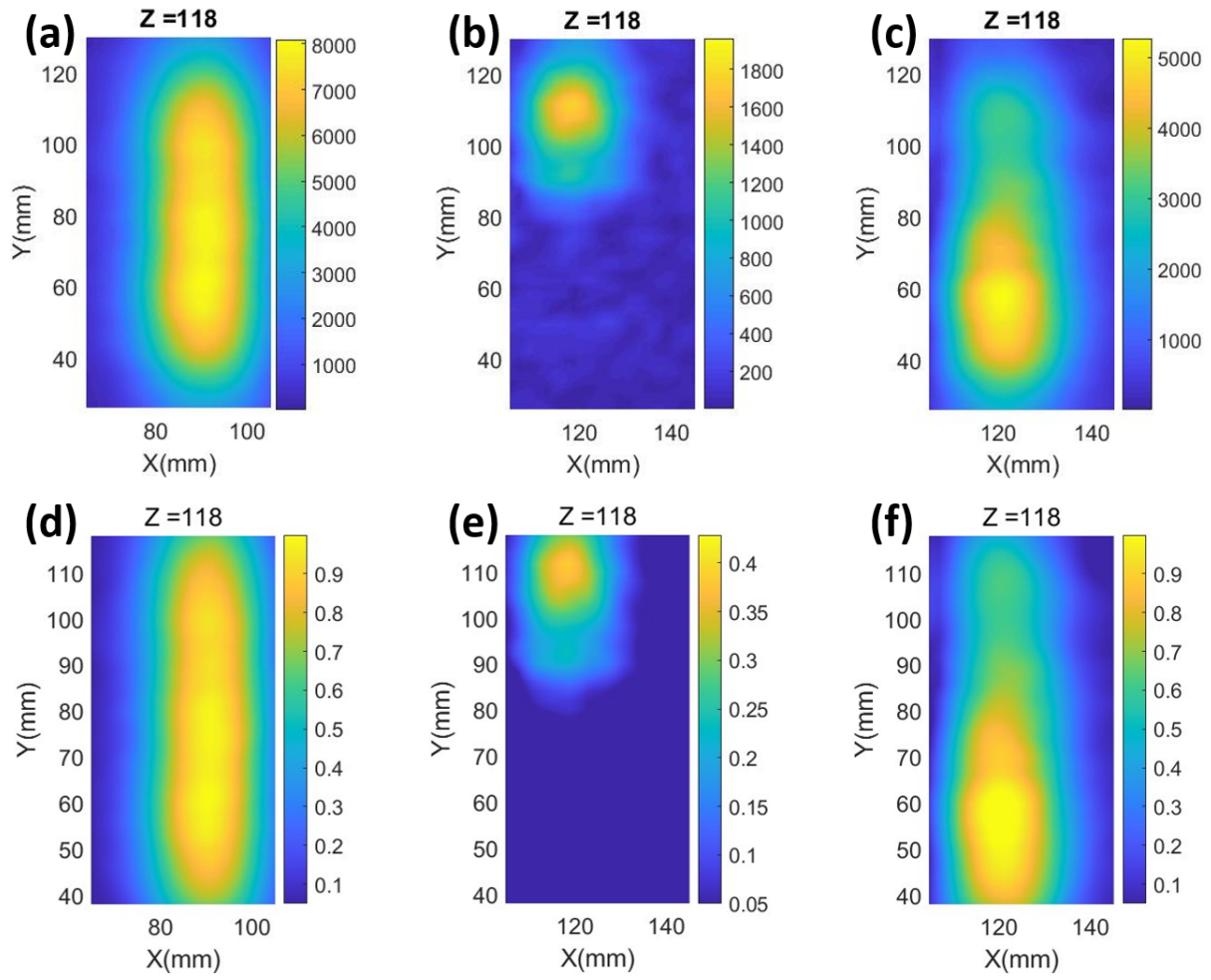
Figure S5. The obtained TA image for water distribution experiment: (a) original image of marker, (b) original image of the first stage, (c) original image of the second stage, (d) estimated water saturation level for marker, (e) estimated water saturation level for the first stage, and (f) estimated water saturation level for the second stage.

Table S1. Water Distribution Imaging Experiment: Water Injected Amount and Time

Separation Between Two Successive Injections

Stage	Injection Number	Time Separation (h)	Injected Amount (mL)
1	1	-	1.5
2	1	2	1.2
	2	2.25	1.2
	3	2.25	1.5